



ISSN: 2785-2997

# Journal of Human, Earth, and Future

Vol. 3, No. 2, June, 2022



## Retrieval of Land Surface Temperature from Landsat-8 Thermal Infrared Sensor Data

Deepak Kumar <sup>1\*</sup>, Anupriya Soni <sup>2</sup>, Manish Kumar <sup>3</sup>

<sup>1</sup> Department of Soil & Water Conservation Engineering, Govind Ballabh Pant University, Pantnagar, India

<sup>2</sup> Department of Environmental Science, Central University of South Bihar-823003, India

<sup>3</sup> College of Agricultural Engineering, Dr. Rajendra Prasad Central Agricultural Univ, India

Received 22 March 2022; Revised 19 May 2022; Accepted 28 May 2022; Published 01 June 2022

### Abstract

Remote sensing technology can be said to be an eye in the sky which provides detailed information on various parameters of the Earth, including climatic, vegetative, and forest variables. For many years, Landsat 8 has been used to study various natural phenomena on Earth. In the present study, Landsat 8 imagery has been used to retrieve land surface temperature (LST). For retrieving LST, TIRS (Thermal Infra-Red Sensor) Spectral Bands have been used. The LST map of Udham Singh Nagar in Uttarakhand, India has been further prepared for the period 2018 to 2021 for the month of October. The result suggested that for the study area, LST varies from 24 °C to 39 °C for the month of October in the aforesaid study period. High temperatures have been observed in built-up areas like towns and residential areas, whereas in agricultural fields and forests, the LST is lower as compared to human-induced built-up areas. Further, the southeastern part of Udham Singh Nagar has higher LST as compared to other regions of the study area.

*Keywords:* Landsat-8; Land Surface Temperature; Udham Singh Nagar; TIRS.

### 1. Introduction

The biggest advantage of remote sensing is that a wide area can be selected for study anywhere in the world and several points can be located in the study area for work without any problems. A series of Landsat satellites (Earth Resources Technology Satellites) were launched, among which the Landsat 8 satellite is the latest. Landsat 8 is one such satellite that has been launched to study natural resource management. Landsat 8 Operational Land Imager (OLI) and Thermal Infrared Sensor (TIRS) images consist of nine spectral bands with a spatial resolution of 30 meters for Bands 1 to 7 and 9. The ultra-blue band is useful for coastal and aerosol studies. Band 9 is useful for cirrus cloud detection, whereas Band 8 is panchromatic, and Band 10 and Band 11 are thematic infrared bands. There are several uses of such remote sensing technology in agriculture and forestry, like irrigation monitoring and management, soil mapping, land cover and degradation mapping, reflectance modelling, determination of water content of a field, water resource mapping, climate change monitoring, air moisture estimation, etc. [1, 2]. Hybrid models of climatic parameters, soil water and groundwater can be prepared by using machine learning techniques coupled with remote sensing [3, 4].

Land Surface Temperature is the radiative skin temperature of land surface, as measured in the direction of remote sensor. LST is estimated by the top of the atmosphere brightness temperature from the infrared spectral channels. Its

\* Corresponding author: [deepak.swce.cot.gbpuat@gmail.com](mailto:deepak.swce.cot.gbpuat@gmail.com)

 <http://dx.doi.org/10.28991/HEF-2022-03-02-02>

➤ This is an open access article under the CC-BY license (<https://creativecommons.org/licenses/by/4.0/>).

© Authors retain all copyrights.

estimation further depends on the albedo, the vegetation cover, and the soil moisture. Land Surface Temperature (LST) is defined as the temperature of the interface between the earth's surface and its atmosphere, and thus it is a critical variable to understanding land-atmosphere interactions and a key parameter in metrological and hydrological studies, which involves energy fluxes [5]. The estimation of LST is important because it has various applications in different fields, like detection of climate change signals, land feedbacks, land cover changes, crop management, water management, fire monitoring, geological applications, etc. Prabhakara et al. (1974) [6] used Nimbus 3 and 4 Iris spectral data in the 11 to 13  $\mu\text{m}$  water vapor window region and further analyzed it to determine the sea surface temperature (SST). The SST derived from this technique agrees with the measurements made by ships to about 10°C. Idso et al. (1977) [7] studied on albedo measurement for remote sensing of crop yields. They have conducted a large area crop inventory experiment (LACIE) and measured reflected solar radiation, which was further used in measuring albedo. Courel et al. (1984) [8] studied the surface albedo and the soil moisture, both of which affect the radiation balance at the surface.

Norman et al. (1995) [9] developed algorithms for extracting information from remote thermal-IR observations of the Earth's surface. They found that thermal infrared observations would continue to play an essential role in partitioning available surface energy into sensible and latent heat components. Pelgrum et al. (2000) [10] researched on surface energy balances of a desert grassland ecosystem. A large volume of both field and remote sensing data has been collected from 1995 to 1998. Airborne Daedalus scanner data with a spatial resolution of 4 m have been used to infer the following land surface characteristics: surface temperature, albedo, and normalized difference vegetation index (NDVI). Stroeve et al. (2001) [11] calibrated surface albedo and surface temperature data for the Polar Regions. Their results suggested that satellite-derived surface albedo values were on an average 10 % less than those measured by the automatic weather stations (AWS). Crow & Wood (2003) [12] has used an Ensemble Kalman filter (EnKF) to assimilate airborne measurements of 1.4 GHz surface brightness temperature acquired during the 1997 Southern Great Plains Hydrology Experiment (SG97) into the TOPMODEL-based Land-Atmosphere Transfer Scheme (TOPLATS). Kay et al. (2003) [13] researched on spatial relationships between snow contaminant content, grain size, and surface temperature from multispectral images of Mt. Rainier, Washington (USA). Sun et al. (2005) [14] worked on retrieving air temperature from land surface temperature. The method was based on thermodynamics. Two important parameters, namely crop water stress index, and aerodynamic resistance were used to build a quantitative relationship between the land surface temperature and the ambient air temperature. Sturm et al. (2005) [15] have observed that changing snow and shrub conditions could affect albedo with global implications. Using measurements and a solar model, they estimate that a land surface transition from shrub-free tundra to shrubland could produce a 69 to 75% increase in absorbed solar radiation during the snow-cover period, depending on latitude.

Yuan & Bauer (2007) [16] compared NDVI and percent impervious surface as indicators of surface urban heat island effects using Landsat imagery. Hall et al. (2009) [17] evaluated surface and near-surface melt characteristics on the Greenland ice sheet using Moderate Resolution Imaging Spectroradiometer (MODIS) and QuikSCAT data. A study by Holmes et al. (2009) [18] using thermal infrared satellite sensors for measuring land surface temperature (TS) was presented. The 37 GHz vertical polarized brightness temperature was used to derive TS because it was considered the most appropriate microwave frequency for temperature retrieval. Patel (2009) [19] estimated LST from Landsat Thermal Images towards Urban Heat Island Mapping of Kolkata. Qin et al. (2001) [20] used the Landsat Thematic Mapper (TM) for studying land surface temperature (LST) from the thermal band data. The study area was the Israel-Egypt border. The result showed that the Israel side did have a significantly higher surface temperature in spite of its denser vegetation cover than the Egyptian side, where bare sand was prevalent. Liang et al. (2010) [21] estimation of land surface radiation and energy budgets from ground measurement, remote sensing, and model simulations. Tedesco et al. (2011) [22] analyzed remote sensing data for the role of albedo and accumulation in the 2010 melting record in Greenland. Summer snowfall was below average for surface mass balance anomalies.

Niclos et al. (2014) [23] analyzed correlations between SAT and geophysical land surface variables, mainly land surface temperature (LST), to establish operative techniques to obtain spatially continuous land SAT maps from satellite data, unlike data provided by meteorological station networks. Rajeshwari & Mani (2014) [24] estimated the LST of Dindigul District using Landsat 8 data. Sharma et al. (2015) [25] developed relationships between biophysical parameters and land surface temperature (LST) in Kolkata city and nearby surrounding areas. Beg et al. (2016) [26] have calculated surface radiance, surface reflectance, surface albedo, NDVI, LAI, surface emissivity, and surface temperature. The selected study area was located in the Tatra Mountains on the borders between Poland and Slovakia. They have suggested temperature of 6.2°C at mountain shadow areas to 34.6°C at bare rocks and bare land area. Ytre-Eide et al. (2017) [27] have worked with the Centre for Environmental Radioactivity (CERAD) project 'UV-maps' to obtain a geographically distributed time-series of solar ultraviolet (UV) radiation in Norway. Anandababu et al. (2018) [28] have estimated LST using Arc GIS over Hosur, Krishnagiri district, Tamil Nadu, India, using LANDSAT-8 satellite data for the period of April and November. Their study was focused on the application of ArcGIS Raster functions and Raster Calculation using LANDSAT-8 for estimating LST. NDVI and LSE were coupled to estimate LST. For further reading on the use of Lst, the following literature may be helpful [29-33].

In the present study, Thermal Infrared Sensor of Landsat-8 has been used to retrieve the LST map of Udham Singh Nagar, Uttarakhand.

## 2. Materials and Methods

### 2.1. Study Area Description

Udham Singh Nagar District is a district of Uttarakhand state in Northern India. The district is located in the Terai region, and is part of Kumaon Division. Udham Singh Nagar has a total area of 2,908 km<sup>2</sup>. The coordinates of this district lies in between 28°N to 58°N and 78°E to 81°E. The locational map of Udham Singh Nagar has been shown in Figure 1.

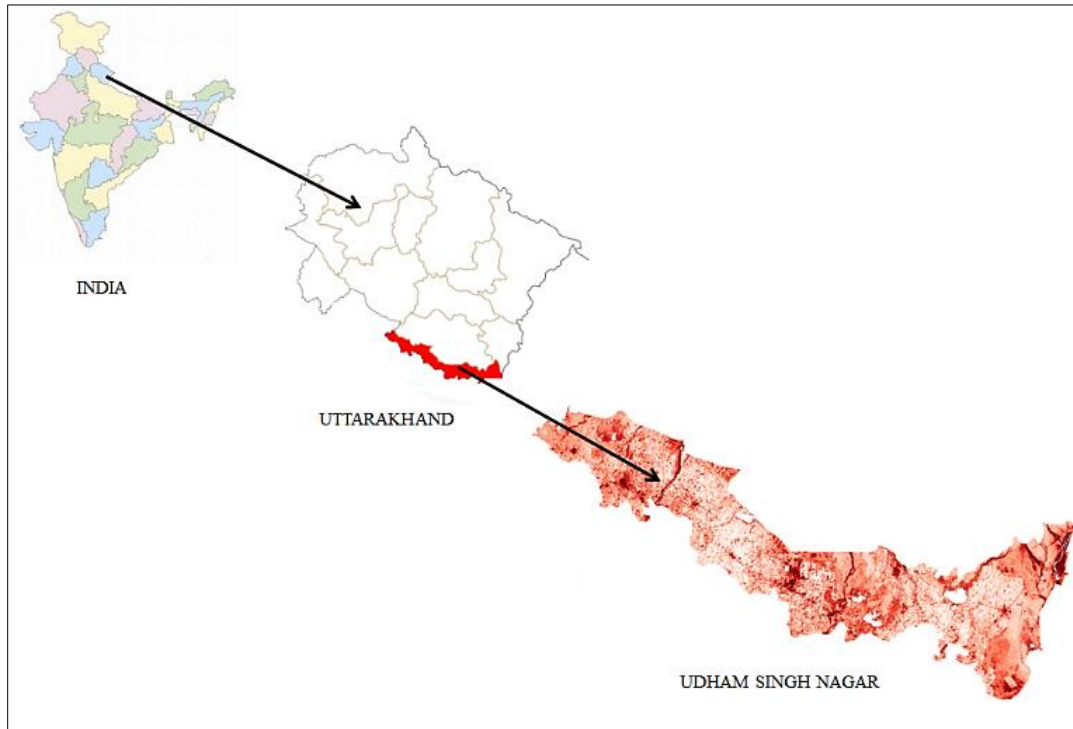


Figure 1. Locational map of study area

For verifying the satellite imagery data with the ground data, CRC Pantnagar, a unit of GBPUAT Pantnagar which record temperature has been selected because the temperature data is available in Pantnagar and it could be easily verified with satellite data.

### 2.2. Sources of Data

Satellite images from LANDSAT-8 OLI/TIRS satellite were used to retrieve surface albedo and land surface temperature. In LANDSAT-8 OLI/TIRS, there are nine OLI spectral bands and two thermal bands which are band 10 and band 11. The Thermal Infrared Sensor (TIRS) measures land surface temperature in two thermal bands with a new technology that applies quantum physics to detect heat. TIRS detect long wavelengths of light emitted by the Earth whose intensity depends on surface temperature. These wavelengths, called thermal infrared, are well beyond the range of human vision. Specification of TIRS has been shown in Table 2.

Table 2. TIRS (Thermal Infra-Red Sensor) Spectral Bands

Spectral Band	Wavelength ( $\mu m$ )	Resolution ( $m$ )
Band 10 - Long Wavelength Infrared	10.30 – 11.30	100
Band 11 - Long Wavelength Infrared	11.50 – 12.50	100

TIRS data from LANDSAT-8 has been collected from 2018 to 2021. To get cloud free image, month of October for study of land surface temperature for the study area has been selected, since remaining seasons may have cloud or partial cloud cover. The revisiting period of LANDSAT-8 is 15 days. Thus, TIRS data can't be obtained daily or weekly. The acquisition dates of the images are given in Table 3.

**Table 3. Image Acquisition dates from LANDSAT-8**

S. No.	Year	Date of image
1	2018	Oct. 27
2	2019	Oct. 14
3	2020	Oct. 16
4	2021	Oct. 19

### 2.3. Estimation of Albedo and Land Surface Temperature

The methods for estimation of albedo and land surface temperature are classified into three main sections. The first section deals with the Atmospheric Correction of Landsat-8 Data. The second section deals with the Calculation of Surface Albedo. Third section deals with the Calculation of Emissivity and Land Surface Temperature.

#### 2.3.1. Atmospheric Correction of Landsat-8 Data

Atmospheric correction for solar radiations is important in remote sensing analysis; its necessity depends on the objectives of the analysis. Estimation of the ground target reflectance starts with converting the pixel value to radiance. Accordingly, Landsat-8 OLI/TIRS bands data can be converted to TOA spectral radiance using the radiance rescaling factors (Equation 1) provided in the metadata of images:

$$L_{\lambda} = ML \times Q_{cal} + AL \quad (1)$$

where,  $L_{\lambda}$  is TOA spectral radiance (Watts/ (m<sup>2</sup>. srad.  $\mu$ m));  $ML$  is Band-specific multiplicative rescaling factor from metadata (Radiance\_Mult\_Band\_x, where x is the band number);  $AL$  is Band-specific additive rescaling factor from the metadata (Radiance\_Add\_Band\_x; x is the band number);  $Q_{cal}$  is Quantized and calibrated standard product pixel values (DN). To compute the top of planetary reflectance Equation 2 has been used:

$$\rho_{\lambda} = \frac{(\pi \times L_{\lambda})}{(ESUN_{\lambda} \times \cos \theta \times d_r)} \quad (2)$$

where,  $\rho_{\lambda}$  is TOA planetary reflectance;  $ESUN_{\lambda}$  is Exoatmospheric spectral solar irradiance on a surface perpendicular to the sun's ray ( $Wm^{-2} * \mu m^{-1}$ );  $\cos \theta$  is solar zenith (90-solar elevation).  $\theta$  is in decimal degree need to be converted into radians using Equation 3:

$$(\theta \text{ in radians}) = \frac{\pi}{180} \times (\theta \text{ in decimal degrees}) \quad (3)$$

$d_r$  = Earth-Sun distance in astronomical calculated using Equation 4.

$$d_r = 1 + 0.033 \times \left( \text{Julian day} \times \frac{2\pi}{365} \right) \quad (4)$$

#### 2.3.2. Calculation of Surface Albedo

The values of albedo for the top of atmosphere were calculated using Equations 5 and 6.

$$\alpha_{toa} = \sum(\omega_{\lambda} \times \rho_{\lambda}) \quad (5)$$

$$\omega_{\lambda} = \frac{ESUN_{\lambda}}{\sum ESUN_{\lambda}} \quad (6)$$

where,  $\omega_{\lambda}$  is Constant value of weighting coefficient. The weighted albedo is converted to surface albedo using Equation 7.

$$\alpha = \frac{\alpha_{toa} - \alpha_{path \text{ radiance}}}{\tau_{sw}^2} \quad (7)$$

where,  $\alpha$  is Surface albedo;  $\alpha_{path \text{ radiance}}$  is incoming shortwave radiation flux reflected back to the sensor range from (0.025 to 0.04).  $\tau_{sw}$  is Atmospheric Transmissivity calculated by Equation 8.

$$\tau_{sw} = 0.75 + 2 \times 10^{-5} \times z \quad (8)$$

where,  $z$  is an elevation of area.

### 2.3.3. Calculation of Emissivity and Land Surface Temperature

To calculate the surface temperature, first the black body temperature at satellite must be calculated using Equation 9.

$$T_b = \frac{K_2}{\ln\left(\frac{K_1}{L_\lambda} + 1\right)} \quad (9)$$

where,  $T_b$  is Blackbody temperature at satellite in Kelvins;  $L_\lambda$  is Spectral radiance in  $W.m^{-2}.ster^{-1}\mu m^{-1}$ ;  $K_1$  And  $K_2$  are calibration constants for Landsat-8 OLI/TIRS thermal band-10. To compute the land surface temperature, the blackbody temperature is corrected with respect to the surface emissivity ( $\epsilon$ ) values. The surface emissivity is a factor that describes the efficiency of an object radiates energy in comparing with black body. The values of emissivity are estimated from NDVI with the help of Equation 10.

$$\epsilon = 1.009 + 0.047 \times \ln(NDVI) \quad (10)$$

where, NDVI is Normalized Difference Vegetation Index which was calculated using Equation 11.

$$NDVI = \frac{Band5 - Band4}{Band5 + Band4} \quad (11)$$

Band 5 is Reflectance of near Infra-Red band; Band 4 is Reflectance of red band. The corrected land surface temperature ( $T_s$ ) is calculated by the Equation 12.

$$T_s = \frac{T_b}{1 + \left(\frac{T_b}{\lambda \times \gamma}\right) \times \ln \epsilon} \quad (12)$$

where,  $\lambda$  is average of limiting wavelengths of band 10 of Landsat8-TIRS ( $\lambda = 10.895\mu m$ ) which was calculated using Equation 13.

$$\gamma = \frac{h \times c}{a} \quad (13)$$

Where,  $a$  = Boltzmann constant ( $1.38 * 10^{-23} j.k$ );  $h$  = Plank's constant ( $6.626 * 10^{-34} J.s$ );  $c$  = velocity of light ( $2.998 * 10^8 m$ )

## 3. Results and Discussion

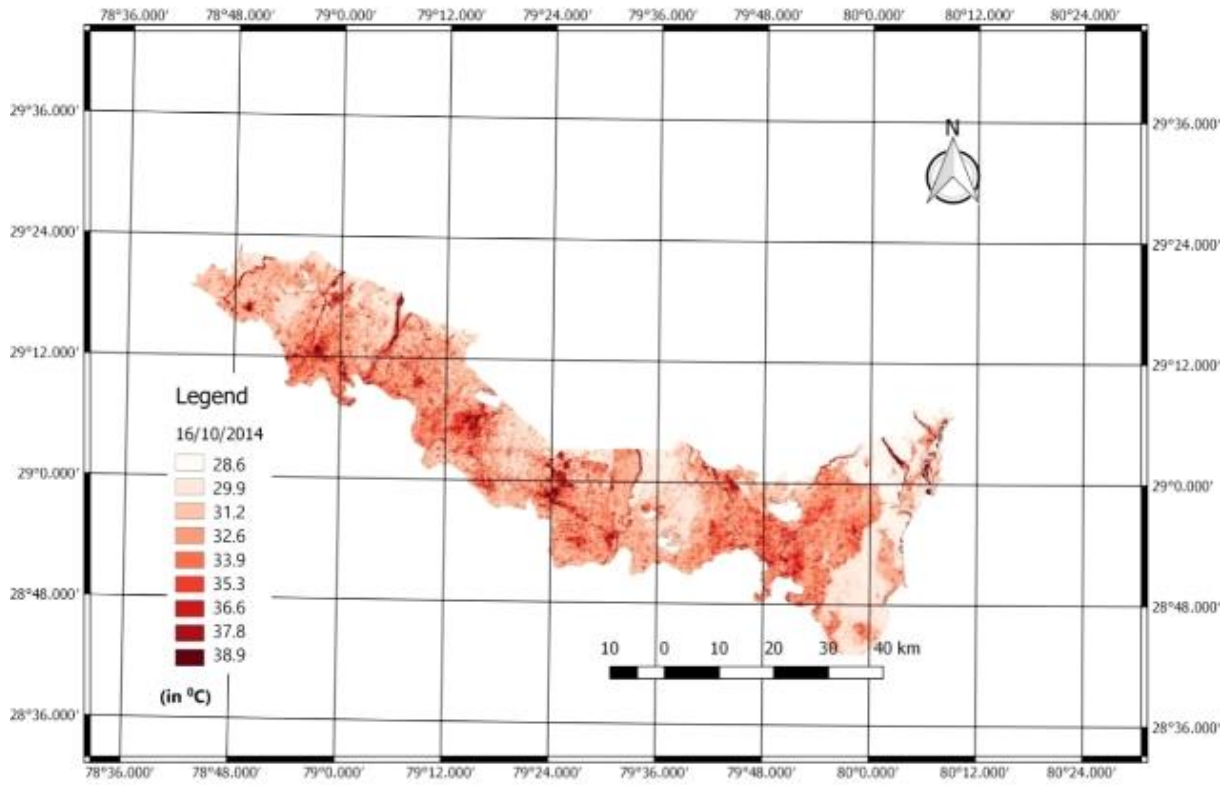
In the present study, LST map of Udham Singh Nagar of Uttarakhand, India has been derived from LANDSAT-8 imagery for the month of October. The images from 2018 to 2021 has been collected whose acquisition dates has been provided in material and method.

For verifying the satellite imagery data with the ground data, CRC Pantnagar has been selected because the temperature data is available in Pantnagar and it could be easily verified with satellite data. The LST data from Landsat 8 and CRC data has been presented in Table 4. Table 4 depicted that difference between LST data collected from ground station and satellite was insignificant ( $\leq 1^\circ C$ ) except for Oct. 14, 2019. The mean LST obtained from satellite data was  $32.85^\circ C$  and mean of ground based LST was  $32.5^\circ C$ . The mean difference between satellite data and actual data was only  $0.35^\circ C$ . The difference in satellite and ground data might be due to the reason that satellite captured the image at a particular time of a day, but at that time hourly data was not available at CRC Pantnagar.

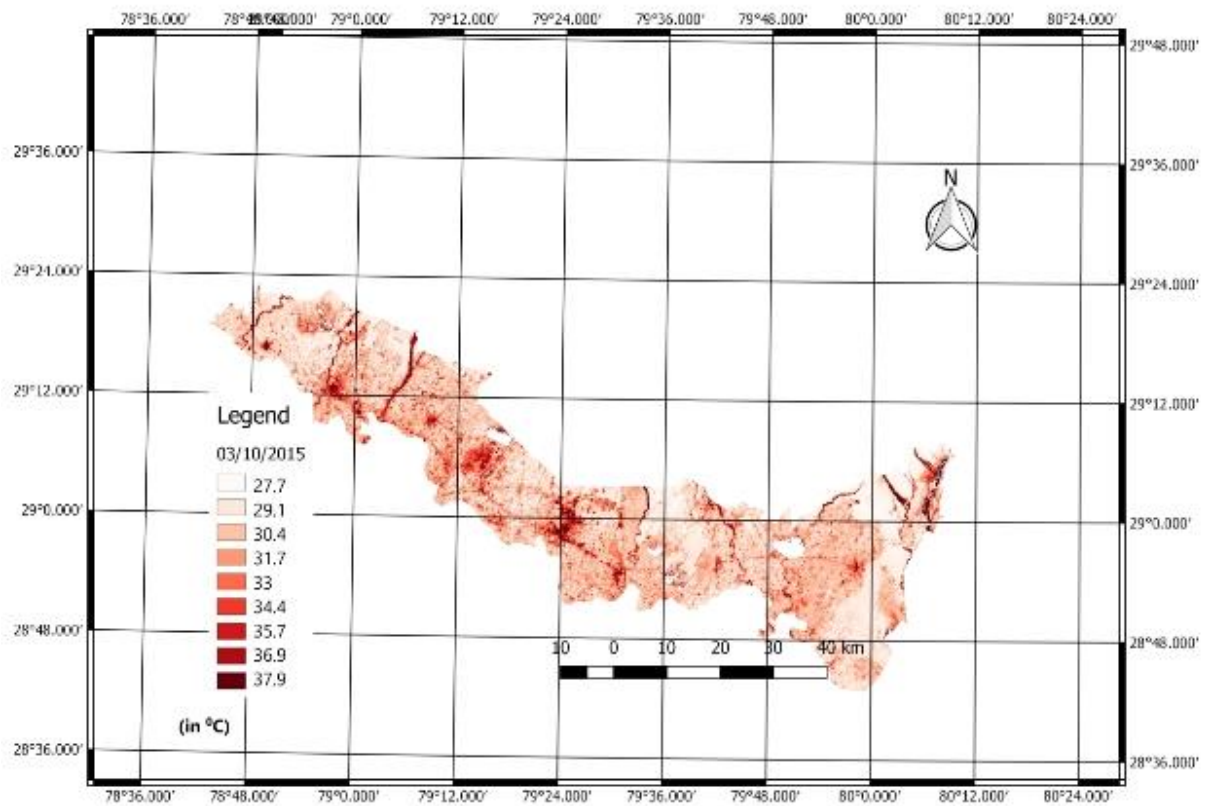
**Table 4. Comparison between actual and satellite retrieved LST**

S. No.	Date of image acquisition	Actual temperature ( $^\circ C$ )	Satellite retrieved LST ( $^\circ C$ )	Absolute Error ( $^\circ C$ )
1	October 27, 2018	32	32.6	0.6
2	14 Oct. 2019	31	32.4	1.4
3	Oct. 16, 2020	34	33.6	0.4
4	19 Oct. 2021	33	32.8	0.4

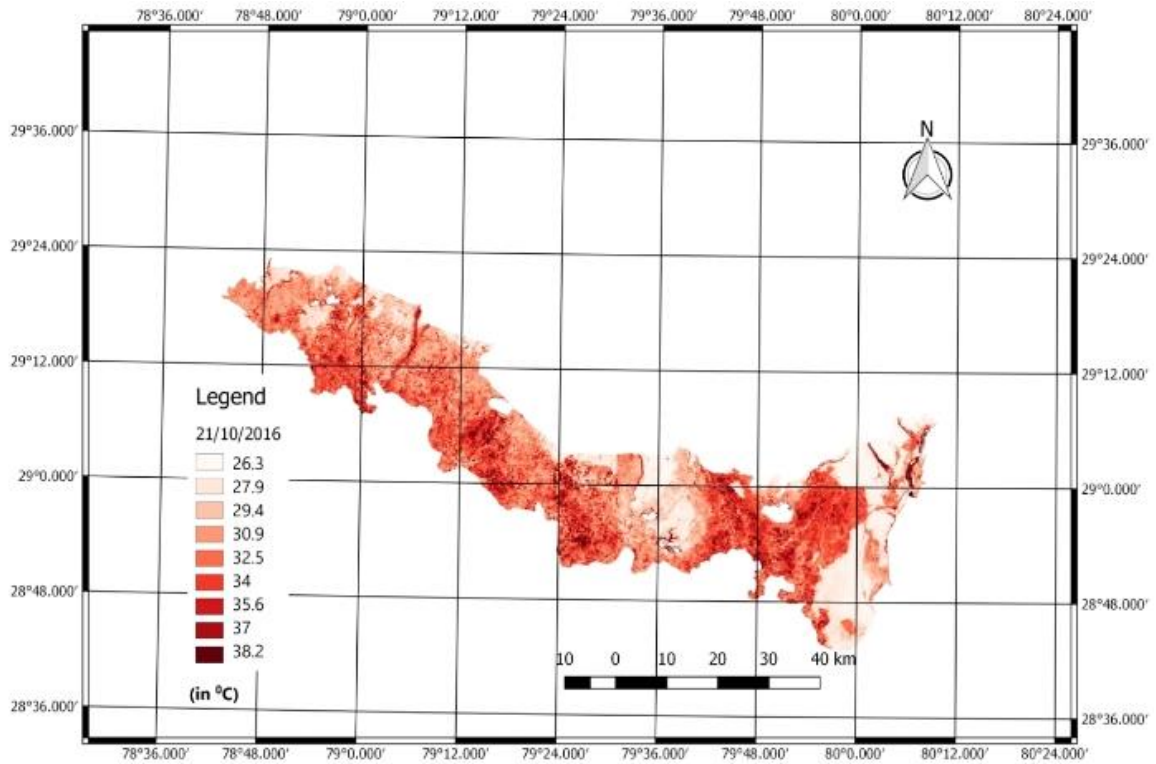
The spatio-temporal patterns of land surface temperature in Udham Singh Nagar district of October from 2018 to 2021 has been shown in Figure 2. The temperature range of study area varies from  $24$  to  $39^\circ C$ . As depicted from Figure 2, spatially 2019 and 2020 were hotter than remaining two years. Moreover, the eastern part of Udham Singh nagar seemed hotter than the remaining.



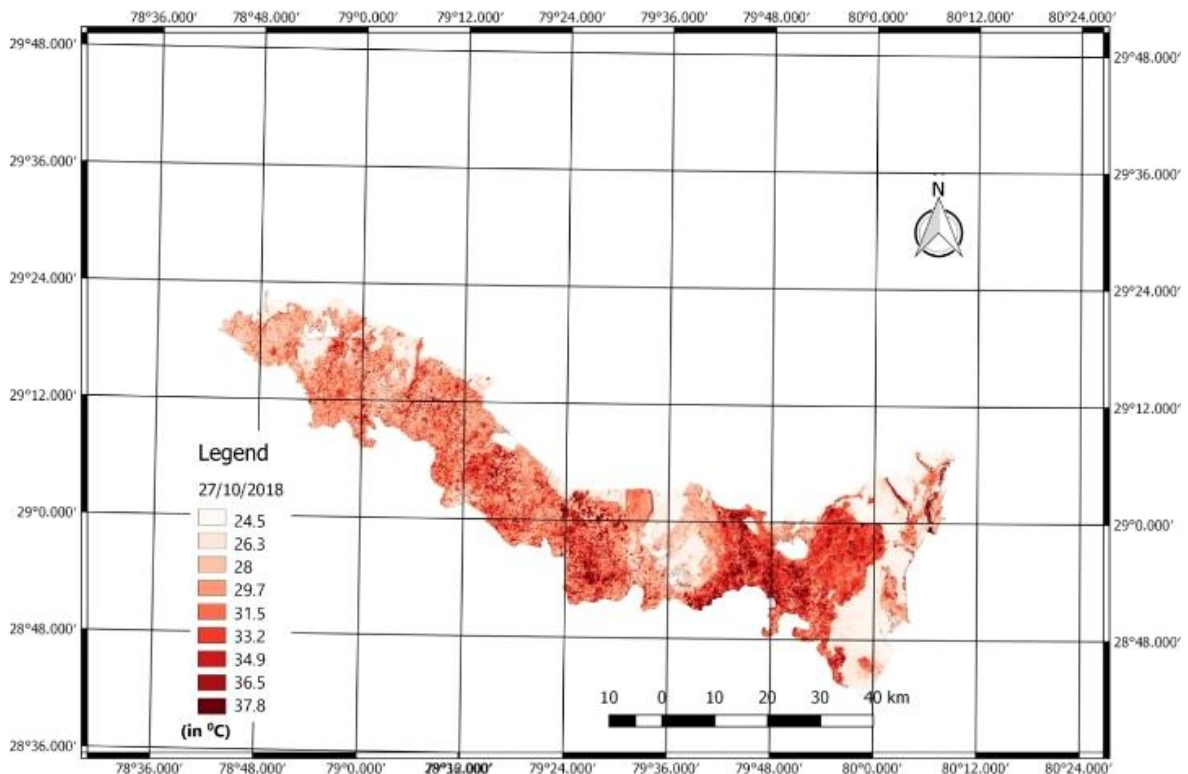
(a) October 27, 2018



(b) October 14, 2019



(c) October 16, 2020



(d) October 19, 2021

**Figure 2. LST map of Udhamsingh Nagar derived from LANDSAT-8 images**

It could be observed from Figure 2 that the LST map for the years 2018, 2019, 2020, and 2021 were not the same. The difference between each year's LST maps could be affected by various factors such as the weather conditions of different days, speed and direction of the wind when the satellite captures the image. Other sources from human activities, e.g., energy consumption from buildings and transportation, can also influence the LST results. However, the most important factors to be considered are the existence of different types of buildings, vegetation, etc.

Further, the images of October from years 2018 to 2019 were merged together to observe the overall spatio-temporal pattern of land surface temperature. It can be observed that most of the areas in the districts were hot in all their central, western, and eastern parts, and all other parts were in the moderate temperature range, except the water bodies.

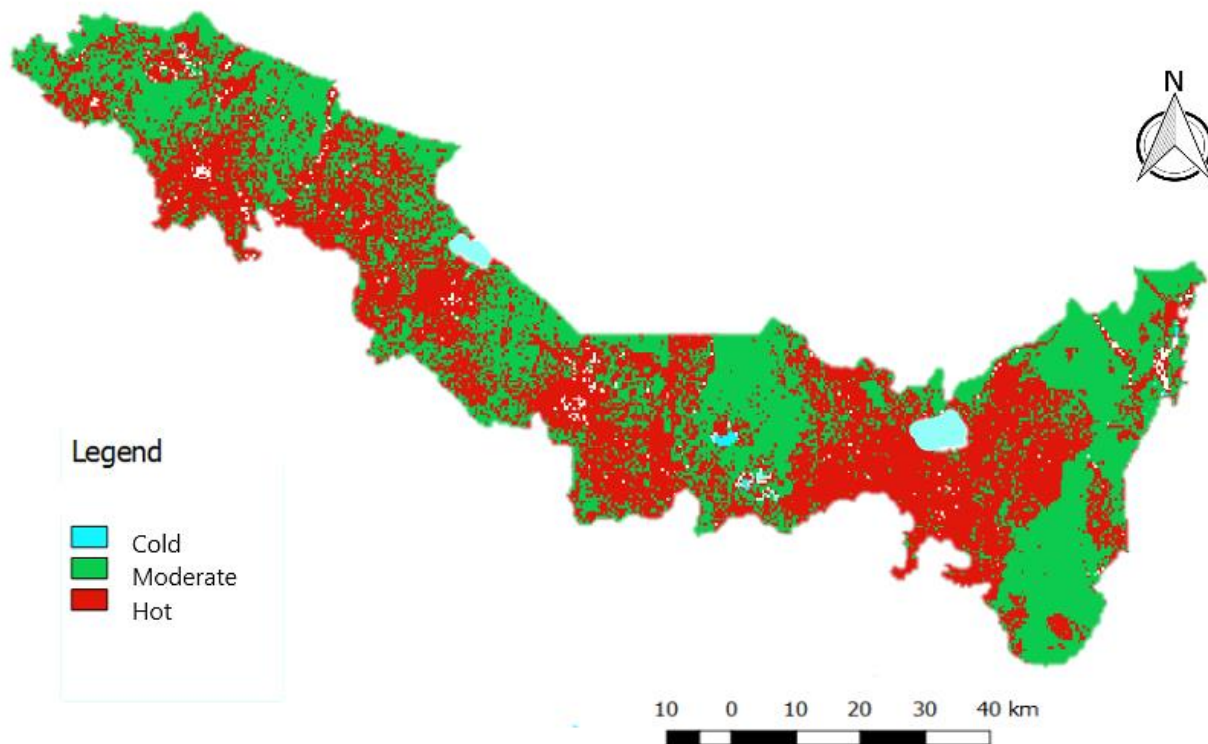


Figure 3. LST Patterns from 2018-2021

In proportion of the total area, most of the area was found to be in the hot temperature range ( $31.7^{\circ}\text{C}$ - $38.9^{\circ}\text{C}$ ), some areas were in the moderate temperature range ( $24.5^{\circ}\text{C}$ - $31.7^{\circ}\text{C}$ ) and the least areas were in the cold temperature range ( $\leq 24.5$ ) of temperature.

#### 4. Conclusion

Remote sensing imagery provides various information about climate, the status of natural resources, and anthropogenic activities going on earth. Anthropogenic activities have caused changes in land use and land patterns, especially in urban areas. Due to remarkable changes in land coverage, the distribution of land surface temperature has also changed. In the present study, remote sensing imagery obtained from the Thermal Infrared Sensor (TIRS) of Landsat 8 has been used to derive land surface temperature (LST). LST is the radiative skin temperature of the land derived from solar radiation. The study area for this study was the Udham Singh Nagar district of Uttarakhand, India. Due to urban development in and around the study area, land use and land patterns have changed remarkably. The LST map of Udham Singh Nagar has been prepared, which could be very helpful to understand the LST temperature distribution in the region. The LST map of the study area suggests that the eastern part of Udham Singh Nagar, which covers the area of Rudrapur, has higher LST as compared to other regions. This also indicates the spread of urban populations in this area.

#### 5. Declarations

##### 5.1. Author Contributions

Conceptualization, D.K.; methodology, A.S.; formal analysis, M.K.; writing—original draft preparation, A.S.; writing—review and editing, D.K. and M.K.; supervision, D.K. All authors have read and agreed to the published version of the manuscript.

##### 5.2. Data Availability Statement

Data available in a publicly accessible repository that does not issue DOIs: Publicly available datasets were analyzed in this study. This data can be found here: [<https://earthexplorer.usgs.gov/>].

### 5.3. Funding

The authors received no financial support for the research, authorship, and/or publication of this article.

### 5.4. Acknowledgements

Authors are thankful to Department of Soil & Water Conservation Engineering for providing the necessary computational facility to carry out this research work.

### 5.5. Institutional Review Board Statement

Not Applicable.

### 5.6. Informed Consent Statement

Not Applicable.

### 5.7. Declaration of Competing Interest

The authors declare that there is no conflict of interests regarding the publication of this manuscript. In addition, the ethical issues, including plagiarism, informed consent, misconduct, data fabrication and/or falsification, double publication and/or submission, and redundancies have been completely observed by the authors.

## 6. References

- [1] Deoli, V., Kumar, D., Kumar, M., Kuriqi, A., & Elbeltagi, A. (2021). Water spread mapping of multiple lakes using remote sensing and satellite data. *Arabian Journal of Geosciences*, 14(21), 1–15. doi:10.1007/s12517-021-08597-9.
- [2] Deoli, V., & Kumar, D. (2020). Analysis of groundwater fluctuation using GRACE satellite data. *Indian Journal of Ecology*, 47(2), 299–302.
- [3] Kumar, D., Adamowski, J., Suresh, R., & Ozga-Zielinski, B. (2016). Estimating Evapotranspiration Using an Extreme Learning Machine Model: Case Study in North Bihar, India. *Journal of Irrigation and Drainage Engineering*, 142(9), 04016032. doi:10.1061/(asce)ir.1943-4774.0001044.
- [4] Kumar, M., Kumari, A., Kumar, D., Al-Ansari, N., Ali, R., Kumar, R., Kumar, A., Elbeltagi, A., & Kuriqi, A. (2021). The superiority of data-driven techniques for estimation of daily pan evaporation. *Atmosphere*, 12(6), 701. doi:10.3390/atmos12060701.
- [5] Niclòs, R., Valiente, J. A., Barberà, M. J., Estrela, M. J., Galve, J. M., & Caselles, V. (2009). Preliminary results on the retrieval of land surface temperature from MSG-SEVIRI data in Eastern Spain. *EUMETSAT 2009: Proceedings of Meteorological Satellite Conference*, January, 21–25, Darmstadt, Germany.
- [6] Prabhakara, C., Dalu, G., & Kunde, V. G. (1974). Estimation of sea surface temperature from remote sensing in the 11- to 13- $\mu$ m window region. *Journal of Geophysical Research*, 79(33), 5039–5044. doi:10.1029/jc079i033p05039.
- [7] Idso, S. B., Reginato, R. J., & Jackson, R. D. (1977). Albedo measurement for remote sensing of crop yields. *Nature*, 266(5603), 625–628. doi:10.1038/266625a0.
- [8] Courel, M. F., Kandel, R. S., & Rasool, S. I. (1984). Surface albedo and the sahel drought. *Nature*, 307(5951), 528–531. doi:10.1038/307528a0.
- [9] Norman, J. M., Divakarla, M., & Goel, N. S. (1995). Algorithms for extracting information from remote thermal-IR observations of the earth's surface. *Remote Sensing of Environment*, 51(1), 157–168. doi:10.1016/0034-4257(94)00072-U.
- [10] Pelgrum, H., Schmugge, T., Rango, A., Ritchie, J., & Kustas, B. (2000). Length-scale analysis of surface albedo, temperature, and normalized difference vegetation index in desert grassland. *Water Resources Research*, 36(7), 1757–1765. doi:10.1029/2000WR900028.
- [11] Stroeve, J. C., Box, J. E., Fowler, C., Haran, T., & Key, J. (2001). Intercomparison between in situ and AVHRR polar pathfinder-derived surface albedo over Greenland. *Remote Sensing of Environment*, 75(3), 360–374. doi:10.1016/S0034-4257(00)00179-6.
- [12] Crow, W. T., & Wood, E. F. (2003). The assimilation of remotely sensed soil brightness temperature imagery into a land surface model using Ensemble Kalman filtering: A case study based on ESTAR measurements during SGP97. *Advances in Water Resources*, 26(2), 137–149. doi:10.1016/S0309-1708(02)00088-X.
- [13] Kay, J. E., Gillespie, A. R., Hansen, G. B., & Pettit, E. C. (2003). Spatial relationships between snow contaminant content, grain size, and surface temperature from multispectral images of Mt. Rainier, Washington (USA). *Remote Sensing of Environment*, 86(2), 216–231. doi:10.1016/S0034-4257(03)00102-0.

- [14] Sun, Y. J., Wang, J. F., Zhang, R. H., Gillies, R. R., Xue, Y., & Bo, Y. C. (2005). Air temperature retrieval from remote sensing data based on thermodynamics. *Theoretical and Applied Climatology*, 80(1), 37–48. doi:10.1007/s00704-004-0079-y.
- [15] Sturm, M., Douglas, T., Racine, C., & Liston, G. E. (2005). Changing snow and shrub conditions affect albedo with global implications. *Journal of Geophysical Research*, 110(G1). doi:10.1029/2005jg000013.
- [16] Yuan, F., & Bauer, M. E. (2007). Comparison of impervious surface area and normalized difference vegetation index as indicators of surface urban heat island effects in Landsat imagery. *Remote Sensing of Environment*, 106(3), 375–386. doi:10.1016/j.rse.2006.09.003.
- [17] Hall, D. K., Nghiem, S. V., Schaaf, C. B., DiGirolamo, N. E., & Neumann, G. (2009). Evaluation of surface and near-surface melt characteristics on the Greenland ice sheet using MODIS and QuikSCAT data. *Journal of Geophysical Research: Earth Surface*, 114(4). doi:10.1029/2009JF001287.
- [18] Holmes, T. R. H., De Jeu, R. A. M., Owe, M., & Dolman, A. J. (2009). Land surface temperature from Ka band (37 GHz) passive microwave observations. *Journal of Geophysical Research Atmospheres*, 114(4). doi:10.1029/2008JD010257.
- [19] Patel, P. P. (2009). Estimation of Land Surface Temperature from Landsat Thermal Images towards Urban Heat Island Mapping of Kolkata. *Asian Studies*, 9(2), 110–200.
- [20] Qin, Z., Karnieli, A., & Berliner, P. (2001). A mono-window algorithm for retrieving land surface temperature from Landsat TM data and its application to the Israel-Egypt border region. *International Journal of Remote Sensing*, 22(18), 3719–3746. doi:10.1080/01431160010006971.
- [21] Liang, S., Liang, S., Zhang, X., Wang, K., Zhang, X., & Wild, M. (2010). Review on Estimation of Land Surface Radiation and Energy Budgets From Ground Measurement, Remote Sensing and Model Simulations. *IEEE Journal of Selected Topics in Applied Earth Observations and Remote Sensing*, 3(3), 225–240. doi:10.1109/JSTARS.2010.2048556.
- [22] Tedesco, M., Fettweis, X., van den Broeke, M. R., van de Wal, R. S. W., Smeets, C. J. P. P., van de Berg, W. J., ... Box, J. E. (2011). The role of albedo and accumulation in the 2010 melting record in Greenland. *Environmental Research Letters*, 6(1), 014005. doi:10.1088/1748-9326/6/1/014005.
- [23] Niclos, R., Valiente, J. A., Barbera, M. J., & Caselles, V. (2014). Land surface air temperature retrieval from EOS-MODIS images. *IEEE Geoscience and Remote Sensing Letters*, 11(8), 1380–1384. doi:10.1109/LGRS.2013.2293540.
- [24] Rajeshwari, A., and Mani, N. D. (2014). Estimation of Land Surface Temperature of Dindigul District Using Landsat 8 Data. *International Journal of Research in Engineering and Technology*, 3(5), 122–126. doi:10.15623/ijret.2014.0305025.
- [25] Sharma, R., Chakraborty, A., & Joshi, P. K. (2015). Geospatial quantification and analysis of environmental changes in urbanizing city of Kolkata (India). *Environmental Monitoring and Assessment*, 187(1), 4206. doi:10.1007/s10661-014-4206-7.
- [26] Ayad Ali Faris Beg, Ahmed H. Al-Sulttani, Adrian Ochtyra, Anna Jarocińska, & Adriana Marcinkowska. (2016). Estimation of Evapotranspiration Using SEBAL Algorithm and Landsat-8 Data—A Case Study: Tatra Mountains Region. *Journal of Geological Resource and Engineering*, 4(6), 257–270. doi:10.17265/2328-2193/2016.06.002.
- [27] Ytre-Eide, M., Christensen, T., Johnsen Istad, T. S., Nilsen, L. T., & Johnsen, B. (2017). Modeling Effective Albedo as a Function of Land Cover Type and Snow Type. In *Free and Open Source Software for Geospatial (FOSS4G) Conference Proceedings 17(1)*: 10. doi:10.7275/R5FJ2F07.
- [28] Anandababu, D., Purushothaman, B.M., and Babu, S.S. (2018). Estimation of Land Surface Temperature using LANDSAT 8 Data. *IJARIT*, 4(2), 312-350.
- [29] Bosco, N. J., & Thomas, M. (2019). Land Surface Temperature Analysis of Kigali City. *Current Journal of Applied Science and Technology*, 32(2), 1–11. doi:10.9734/cjast/2019/45426.
- [30] Winton, M. (2006). Amplified Arctic climate change: What does surface albedo feedback have to do with it? *Geophysical Research Letters*, 33(3). doi:10.1029/2005GL025244.
- [31] Peng, J., Fan, W., Xu, X., Wang, L., Liu, Q., Li, J., & Zhao, P. (2015). Estimating crop Albedo in the application of a physical model based on the law of energy conservation and spectral invariants. *Remote Sensing*, 7(11), 15536–15560. doi:10.3390/rs71115536.
- [32] Sánchez, J. M., Caselles, V., Niclòs, R., Coll, C., & Kustas, W. P. (2009). Estimating energy balance fluxes above a boreal forest from radiometric temperature observations. *Agricultural and Forest Meteorology*, 149(6–7), 1037–1049. doi:10.1016/j.agrformet.2008.12.009.
- [33] Tang, R., Li, Z. L., Jia, Y., Li, C., Chen, K. S., Sun, X., & Lou, J. (2013). Evaluating one- and two-source energy balance models in estimating surface evapotranspiration from Landsat-derived surface temperature and field measurements. *International Journal of Remote Sensing*, 34(9–10), 3299–3313. doi:10.1080/01431161.2012.716529.